J Mol Model (2012) 18:3915–3926
DOI 10.1007/s00894-012-1396-1

ORIGINAL PAPER

Theoretical study of the decomposition mechanisms and kinetics of the ingredients RDX in composition B

Jian-Guo Zhang · Kun Wang · Xiao-Qing Niu · Shao-Wen Zhang · Xiao-Jun Feng · Tong-Lai Zhang · Zun-Ning Zhou

Received: 11 October 2011 / Accepted: 28 February 2012 / Published online: 20 March 2012

Abstract RDX as a component in composition B (TNT + RDX) was first studied by us on its mechanism and kinetics of decomposition reactions in this paper. We have pointed out three possible pathways and found a new low-energy process of its decomposition. The N—N bond cleavage in composition B has higher dissociation energies than the monomer, but it is also the initial step. The optimized structures and the frequencies of all the stationary points were calculated at the B3LYP/6-31G(d) level. The minimum-energy paths were obtained by using the intrinsic reaction coordinate (IRC) theory, and the reaction potential energy curve was corrected with zero-point energy. Finally, the rate constants were calculated in a wide temperature region from 200 to 2500 K using TST, TST/Eckart theories. The obtained results also indicate that the tunneling effects are remarkable at low temperature (200 K <T < 500 K).

Keywords Composition B (TNT + RDX) · Decomposition mechanisms · Kinetics · Potential energy surface · Rate constants · Transition state

J.-G. Zhang (✉) · K. Wang · X.-Q. Niu · T.-L. Zhang · Z.-N. Zhou
State Key Laboratory of Explosion Science and Technology,
Beijing Institute of Technology,
Beijing 100081, People's Republic of China
e-mail: zhangjianguobit@yahoo.com.cn

S.-W. Zhang
School of Science, Beijing Institute of Technology,
Beijing 100081, People's Republic of China

X.-J. Feng
Xi'an Modern Chemistry Research Institute,
Xi'an 710065, People's Republic of China

Introduction

Composition B is a kind of high-energy explosive, which is made up of 2,4,6-trinitrotoluene (TNT) and hexahydro-1,3,5-trinitro-1,3,5-triazine (RDX). It has been widely used because of its outstanding physical property. Because of the high-sensitivity of RDX, the main component of composition B, it is meaningful to discuss composition B security by thermal sensitivity test, mechanical sensitivity test and theoretical study [1, 2]. Many theoretic and sensitive studies have been concentrated on the decomposition of monomer RDX recently. Experimental studies of RDX were mainly focused on the condensed phase. Experimental evidence indicates that the decomposition of RDX is a complex process in different conditions [3, 4]. Melius and Binkley [5] studied the decomposition mechanism in the gas phase by using BAC-MP4 level of ab initio method. Harris and Lammmertsma [6] pointed out that the N—N and C—H are the weakest bonds in RDX by using the density functional method (B3LYP). Wu and Fried [7] studied two decomposition pathways of RDX which are the dissociation of N—N bond and the concerted ring by using DFT methods. Chakraborty and Muller [8] discussed the monomer decomposition mechanism of RDX by using B3LYP/6-31G(d) level and indicated three ways of its initio decomposition, which are the concerted HONO elimination, the breaking of N—N bond and the concerted ring. Boyd et al. [9, 10] have developed a new model for molecular dynamics/ Monte Carlo simulation of formation, diffusion and agglomeration of point defects in the crystal lattice of α-RDX and investigated the factors of detonation initiation of energetic material. All in all, these theoretical and experimental studies suggested that the N—N hemolytic cleavage is the key of the decomposition. However, there are few reports about the RDX in the mixture (e.g., composition B). We first studied

the intermolecular interactions in composition B and obtained some meaningful information in the recent work [11]. Interactions of hydrogen bonds between the components contribute to the changes of properties from monomers to complexes. In this study, DFT method was used to study the mechanism and transition states of each decomposition step. Furthermore, the rate constants are calculated at the temperature ranged from 200 to 2500 K. The theoretical results of the mixture was compared with that of monomer decomposition of RDX.

Methods

All calculations were carried out by using DFT methods by Gaussian 03 program [12]. The optimized structures and the frequencies of all the stationary points (reactants, products and transition states) were calculated at the Becke three parameter hybrid density functional method with the Lee-Yang-Parr correlated functional approximation(B3LYP) [13] in the 6-31G(d) basis set. This level of theory was shown to be adequate for the detonation mechanism of large molecular systems such as RDX [2–4]. The minimum-energy paths are insured by using the intrinsic reaction coordinate (IRC) theory [14] at the same level of theory with the step length 0.02 $(amu)^{1/2}$·bohr. And the reaction potential energy curve is corrected with zero-point energy. Finally, the rate constants are obtained at a wide temperature region from 200 to 2500 K with conventional transition-state theory (TST) [15], the TST rate constant calculations with the Eckart tunneling correction theory (TST/Eckart) [16] by using the online Vklab program package [17] and POLYRATE 8.2 program [18].

Results and discussion

Geometries and energies

In this paper, three distinct initial decomposition pathways have been identified for RDX in composition B (TNT + RDX), similarly. The fist pathway is initiated with N—NO_2 breaking and then it undergoes further decomposition with four different pathways. A new way expressed by d has been shown here (Scheme 1). The second pathway is initiated by an HONO elimination reaction (Scheme 2). The third pathway is the dissociation of the ring (Scheme 3). The optimized structures and some bond parameters for reactants, products and transition states (TS) of composition B are given in Fig. 1. The vibrational frequencies are calculated to confirm the character of stable point and to correct the zero point energy. The frequencies of all the reactants and products are positive, which proves they are the stable points on the potential energy surface. We also designed the different transition state of each reaction and optimized them. The only imaginary frequency of them mean the designations are reasonable. And the data has been shown in Fig. 1.

The data in Fig. 2 shows the corresponding energy variation of those paths. The reaction enthalpy (ΔG^{θ}_{298K}), free energy (ΔH^{θ}_{298K}) and the reaction energies ($^{\triangle}$E) for the reactions as calculated at the same level of theory were shown in Table 1.

(1) *N—NO_2 fission pathway*

The N—NO_2 bond is believed to be the weakest bond in RDX [6], but the associated endothermicity for further decomposition makes this pathway less favorable. There are four possible energy pathways in this reaction (Scheme 1).

Path a: (1) RDX in composition B will change to RDR after losing one molecule of NO_2. The energy of that is 169.25 kJ mol^{-1}. From Fig. 2 we can see that initiation of the decomposition occurs through the N—NO_2 bond dissociation. Here, Melius and Binkley [5] had predicted the values of the N—NO_2 bond dissociation energy of RDX have ranged from 146.3 to 200.6 kJ mol^{-1}. The research of Wu and Fried [7] and Chakraborty [8] had predicted the dissociation energies of monomer are 142.96 and 163.02 kJ mol^{-1} respectively. So our result is in a permissible range and slightly larger than the values of monomer since the influence of TNT. (2) The follow-up step is the dissociation of C—N bond between –CH_2 and –N-NO_2, and the molecular becomes a chain structure (RDR-o) after the transition state TS1. The barrier and reaction energies ($^{\triangle}$E) of this step are 103.91 and 69.14 kJ mol^{-1} respectively. (3) Isomeric product INT1 is a production with H migration after TS2. The barrier and $^{\triangle}$E of this step are 47.58 kJ mol^{-1} and −5.82 kJ mol^{-1}, which indicate that the isomeric INT1 is more stable than RDR-o. (4) IN1 is an isomer of RDR, which is obtained to form a more stable product INT2 by eliminating HCN (TS3) from RDR-o. The barrier and $^{\triangle}$E is 47.37 and −25.47 kJ mol^{-1}. (5) The bond length of C—N in INT2 between methylenenitramine and nitrogen atom is 1.364 Å, which is similar than that of C=N. While the bond length of the other side between –CH_2 and –NH is 1.437 Å, and the distance between –N-CH_2 and –CH_2-NH is 1.476 Å which is similar to the single bond length of C-N, and it indicates the last one is the weakest bond of the three. Therefore INT2 can be easily turned to MNH and MN passed by TS4, the barrier and $^{\triangle}$E is 119.33 and 106.01 kJ mol^{-1}.

Path b: (6) The C—N bond in RDR-o breaks to form MN molecule and INT3 with a barrier and $^{\triangle}$E of 113.17 and 87.79 kJ mol^{-1}. (7) Finally, INT3 decomposes to the ultimate product CH_2N and MN passed by the TS6. The barrier

Scheme 1 The process for N—NO_2 fission pathway

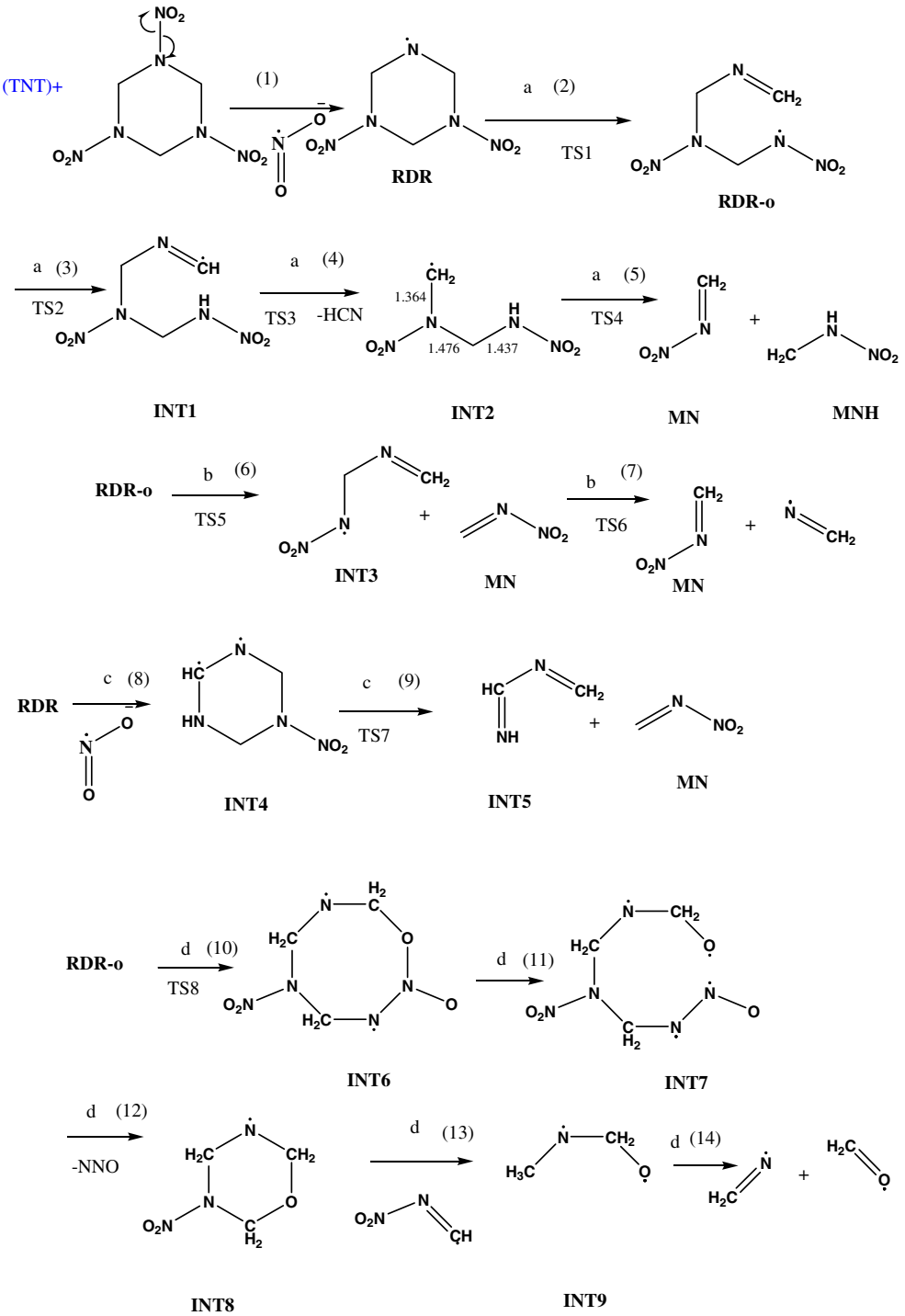

and △E of this step are 48.48 and 56.75 kJ mol^{-1}, which is maximal energy in all products.

Path c: (8) RDR goes to a stable product INT4 with △E of −105.95 kJ mol^{-1}. The INT4 then further decomposes to INT5 and MN after conforming TS7 with a barrier of 247.01 kJ mol^{-1}.

Path d: The final products of those pathways agreed with the experimental behavior: (10) A ring has been formed, a steady eight member ring (INT6) from RDR-o between the O atom of -NO_2 and the nearby C atom of=CH_2 by an addition reaction. The barrier of TS8 and △E of the reaction are 117.95 and 60.81 kJ mol^{-1}. Then the bond O—N in the ring of INT6 breaks to form INT7. INT7 loses an NNO to form a more stable product INT8 with low energy of −300.79 kJ mol^{-1}. INT8 loses a MN molecule to form INT9. Finally, INT9 decomposes to the ultimate product CH_2N and CH_2O.

Scheme 2 The process for HONO elimination pathway

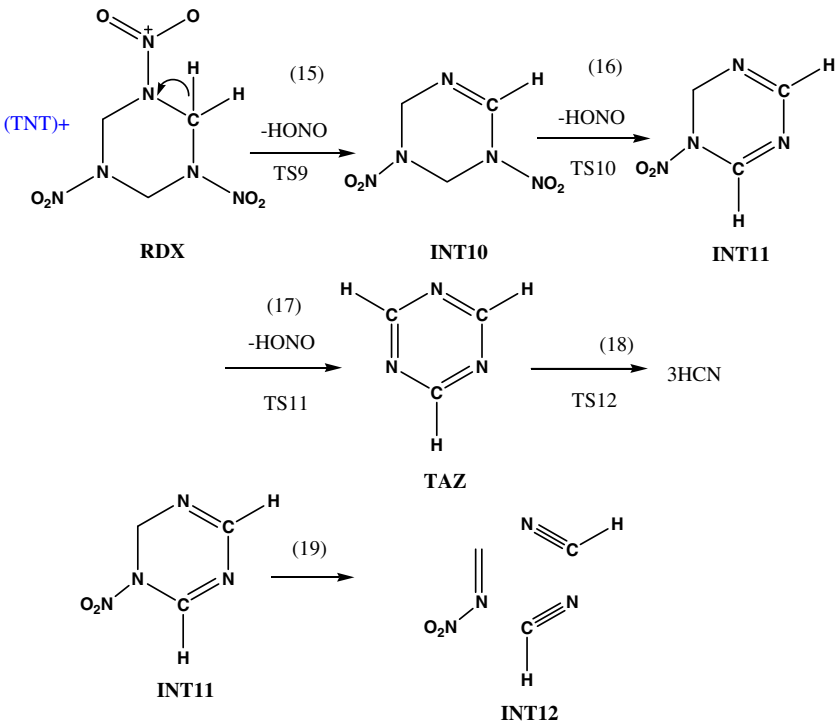

The bond lengths between C and N atoms of TS1, TS3, TS4, TS5, TS6 and TS7 are 2.145, 1.828, 2.259, 2.508, 1.971 and 2.000 Å, which is obviously larger than a typical C—N single bond (1.472 Å), so we can see the distance between C and N is longer and longer with the proceeding of the reaction. TS2 is an ordered seven-membered ring with the H of CH_2 positioned between the C of CH_2 and the N—NO_2 in distances of 1.274 and 1.364 Å. The distance between O and N of TS8 is 1.961 Å, which is close to the single bond length of N—O. The distance between C and O atoms of TS9 is 1.961 Å, which is also close to a typical single bond bond length of C—O (1.440 Å), so the C—O single bond will be formed. So it indicates that the transition states are designed appropriately and indeed connect with the reactant and products.

Table 1 shows that ΔG^{θ}_{298K} and ΔH^{θ}_{298K} of the reaction (8) are both negative, which indicated that it is an exothermic and spontaneous reaction theoretically. Therefore, path c might be the key step among the N—NO_2 dissociation pathways.

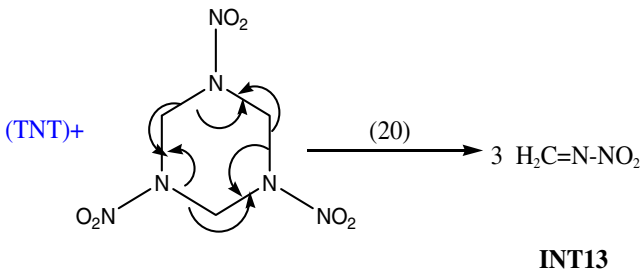

Scheme 3 The process for the concerted ring cleavage pathway

(2) *HONO elimination pathway*

Here we find another pathway to be more favorable than the N—NO_2 dissociation pathway discussed above. According to Scheme 2, at the initial step (15), one O atom of -NO_2 group connects to the H atom of a nearby -CH_2 group for the first HONO elimination to form INT10. The calculated barrier of this step is 193.77 kJ mol^{-1}, which is larger compared to the monomer [8] about 30 kJ mol^{-1} because of the intermolecular interactions of TNT + RDX and the effect of hydrogen bond can not be neglected. The $\triangle$E of this step is −5.48 kJ mol^{-1}, which means that INT10 is a stable structure and hard to dissociate. (16) INT10 elimination the second HONO to form INT11. The barrier and $\triangle$E of it are 184.44 and −12.16 kJ mol^{-1}. The energy of the product INT11 is lower than composition B. (17) INT11 can subsequently eliminate the third -HONO group to form a more stable intermediate TAZ. The barrier of TS11 is 160.28 kJ mol^{-1}. (19) INT11 can also decompose into INT12 directly and the $\triangle$E of it is 153.67 kJ mol^{-1}. (18) TAZ is a very stable product, but it can also decompose into three HCN through the TS12 with a high barrier and $\triangle$E which are 390.85, 197.28 kJ mol^{-1} respectively.

The bond length of N—N of TS10, TS11, TS12 are 2.086, 2.127 and 2.245 Å, and the bond length of C—H are 1.345, 1.332 and 1.240 Å respectively, whereas the

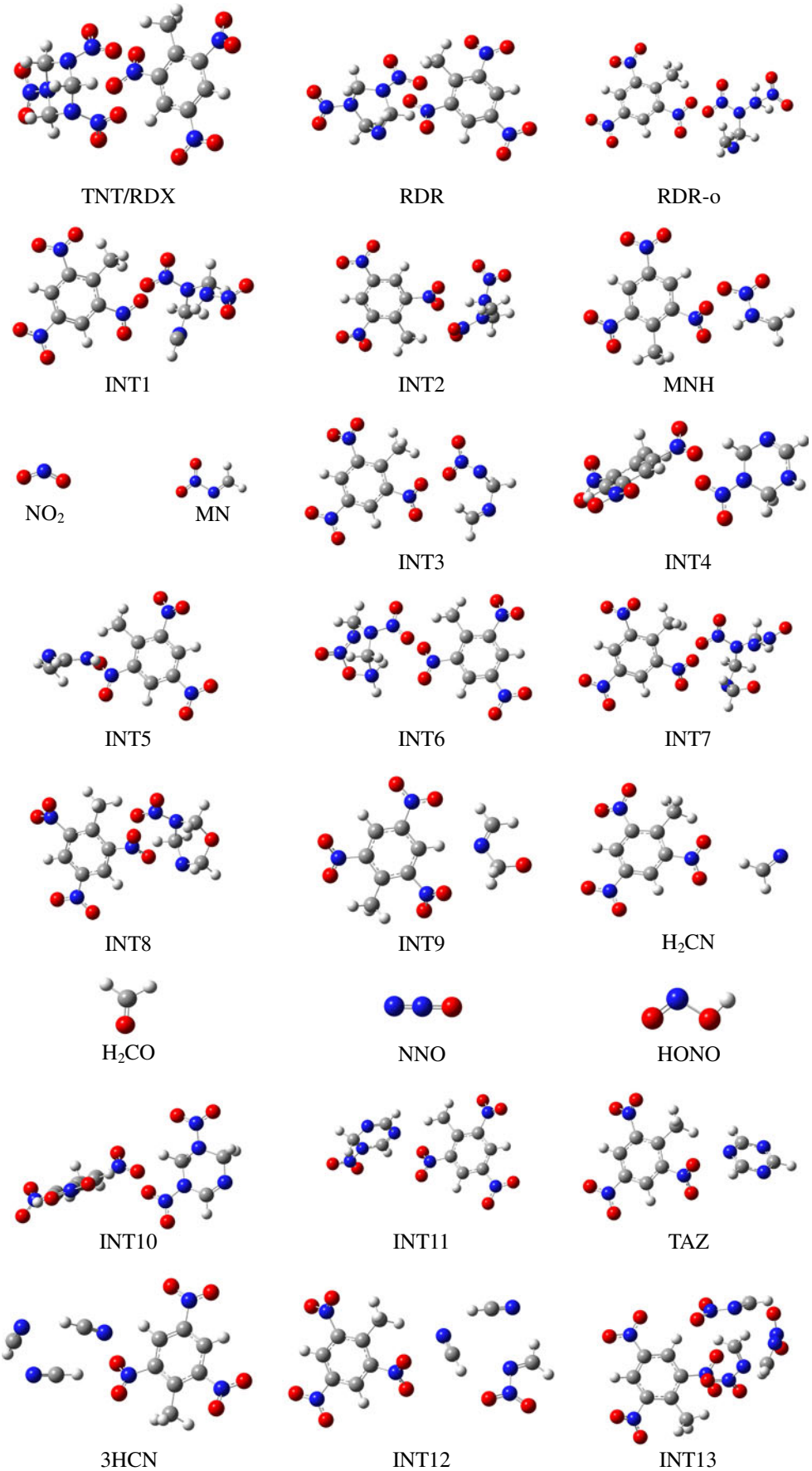

Fig. 1 The geometries of all the stationary points of TNT + RDX for the reaction using B3LYP/6-31G(d) level of theory

Fig. 1 (continued)

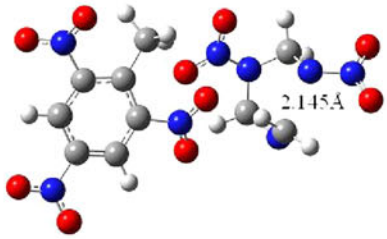

TS1(***371i***)

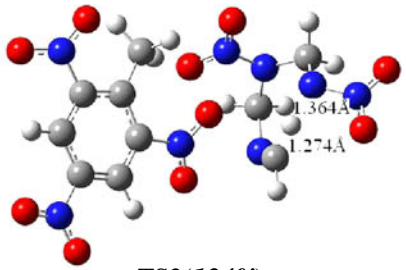

TS2(***1340i***)

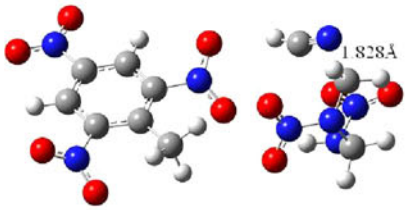

TS3(***675i***)

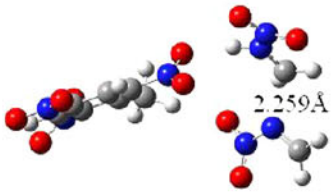

TS4(***278i***)

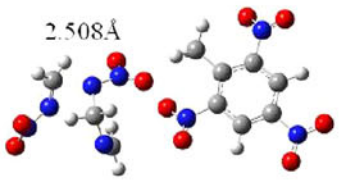

TS5(***389i***)

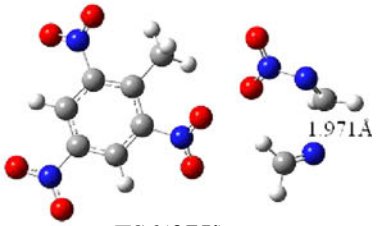

TS6(***375i***)

TS7(***217i***)

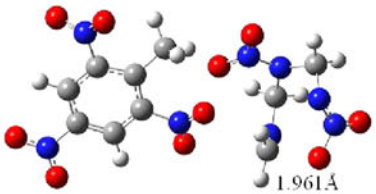

TS8(***660i***)

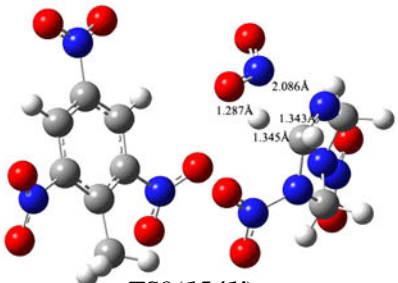

TS9(***1541i***)

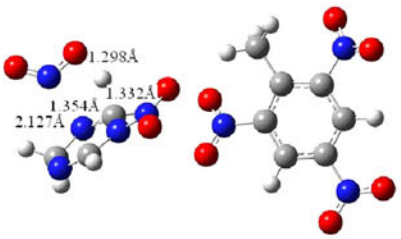

TS10(***1525i***)

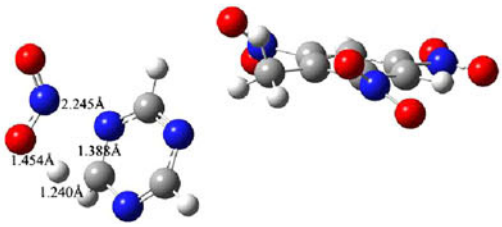

TS11(***991i***)

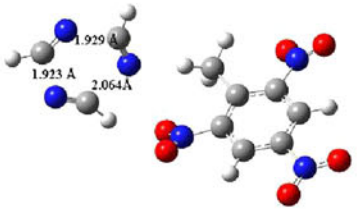

TS12(***602i***)

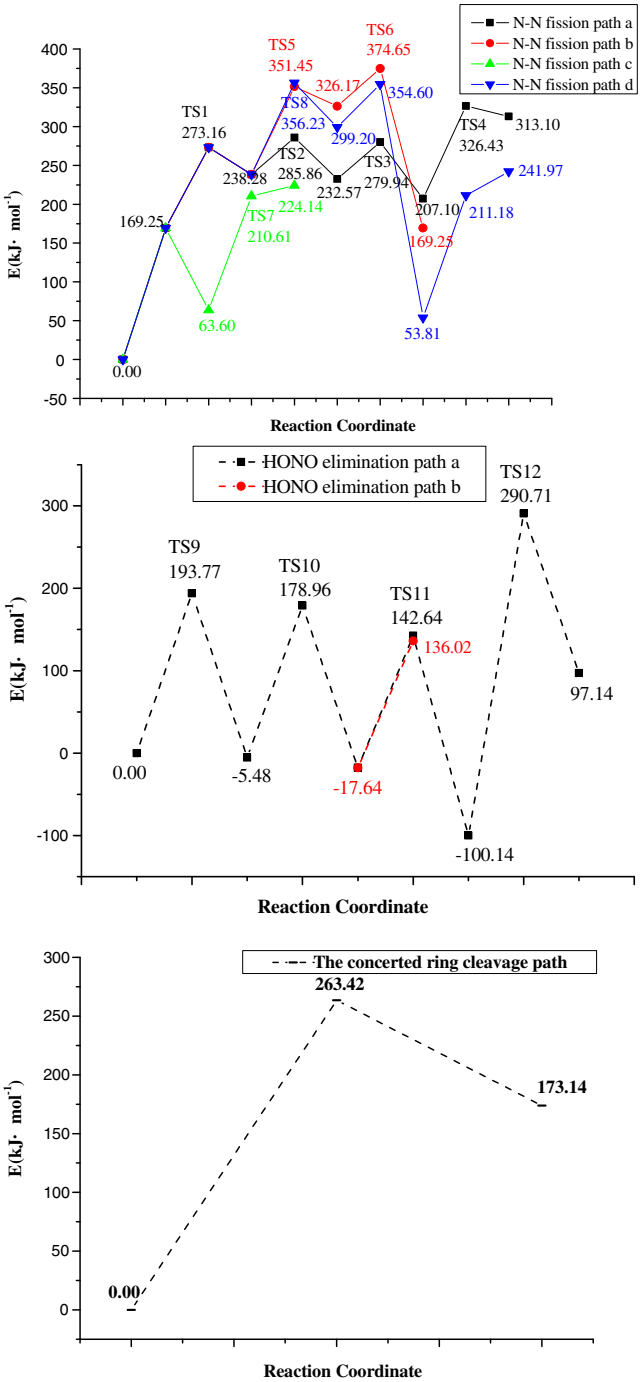

Fig. 2 Potential energy surface of the reactions as calculated at the B3LYP/6-31G(d) level of theory

distance of the new bond O—H are 1.287, 1.298 and 1.454 Å. The length of new C-N bonds of the three are 1.343, 1.335 and 1.388 Å. Due to the elimination of HONO, which impacts the adjacent -NO_2 rearranges from axial to equatorial orientation. The bond lengths of C—H in TS12 are 1.929, 2.064 and 1.923 Å, which is obviously larger than the single bond length of C—H (1.337 Å), while the angles of H—C—N in TS12 are 143.35°, 142.80° and 149.71°, which are close to each other.

The data in Table 1 showed that ΔH^{θ}_{298K} is negative and ΔG^{θ}_{298K} is positive for the reactions (15), (16) and (17), which indicated that they are exothermic and non-spontaneous reactions theoretically. Therefore, the -HONO elimination pathway is the most exothermic primary decomposition channel. However, the calculated entropy of this step is positive. As a result, the Gibbs free energy of the pathway will decrease and this pathway will become spontaneous at elevated temperatures.

(3) *The concerted ring cleavage pathway*

According to Scheme 3, the ring dissociates to three molecular (MN). The barrier of this step is 263.42 kJ mol^{-1}, which is larger than the value of monomer [8]. The result [3] indicates that if the barrier is more than 160 kJ mol^{-1}, then this pathway is not the best one of the three. The preferred pathway must be the one we discussed above.

The data in Table 1 shows that ΔH^{θ}_{298K} and ΔG^{θ}_{298K} of this pathway are both positive, which indicated that it is an exothermic and non-spontaneous reaction. The entropy of

Table 1 The reaction energies, enthalpy and Gibbs free energy for the reactions calculated at the B3LYP/6-31G(d) level of theory (kJ mol^{-1})

N—NO_2 Fission pathway				
Reactions		ΔE	ΔG^{θ}_{298K}	ΔG^{θ}_{298K}
Path a	(1)	169.25	−46.69	107.59
	(2)	69.14	6.51	173.24
	(3)	−5.82	8.23	172.07
	(4)	−25.47	−44.24	159.28
	(5)	106.01	30.81	296.28
Path b	(6)	87.79	33.18	288.80
	(7)	56.75	92.91	381.77
Path c	(8)	−105.95	−346.51	−48.72
	(9)	160.84	−226.62	131.21
Path d	(10)	60.81	79.16	227.49
	(11)	55.40	109.68	273.02
	(12)	−300.79	−177.46	23.14
	(13)	157.36	−66.31	202.22
	(14)	30.80	−68.10	262.51
HONO elimination pathway				
Reactions		ΔE	ΔH^{θ}_{298K}	ΔG^{θ}_{298K}
(15)		−5.48	−35.03	32.55
(16)		−12.16	−73.68	47.12
(17)		−82.50	47.47	169.19
(18)		197.28	−206.26	−2.74
(19)		153.67	27.75	174.40
The concerted ring cleavage pathway				
Reactions		ΔE	ΔH^{θ}_{298K}	ΔG^{θ}_{298K}
(20)		173.14	122.76	167.13

this step is positive. So it is similar to the second one we have talked about.

Reaction properties

The minimum energy path from reactant to products was scanned by IRC calculation which identified if the simulant transition state is credible. In addition, 100 points had been selected on the MEP which would be calculated on the same level to obtain the energy parameters, including gradients and the Hessian matrix at geometries. Figure 3 shows the classical potential barriers ($V_{MEP} = E_{ts} - E_{reactants}$) and the vibrationally adiabatic ground state potential energy curve (V_a^G).

TS1, TS3, TS4, TS5, TS6, TS7, TS8 and TS12 in Fig. 3 have been showed that the curves are smoother and their imaginary frequencies are smaller (371i cm^{-1}, 675i cm^{-1}, 278i cm^{-1}, 389i cm^{-1}, 375i cm^{-1}, 217i cm^{-1}, 660i cm^{-1} and 602i cm^{-1}), while the curves of hydrogen-transfer reaction TS2, TS9, TS10 and TS11 are sharper with larger imaginary frequencies (1340i cm^{-1}, 1541i cm^{-1}, 1525i cm^{-1} and 991i cm^{-1}). So we can infer that the smaller the imaginary frequencies are, the smoother the curves are, this type of

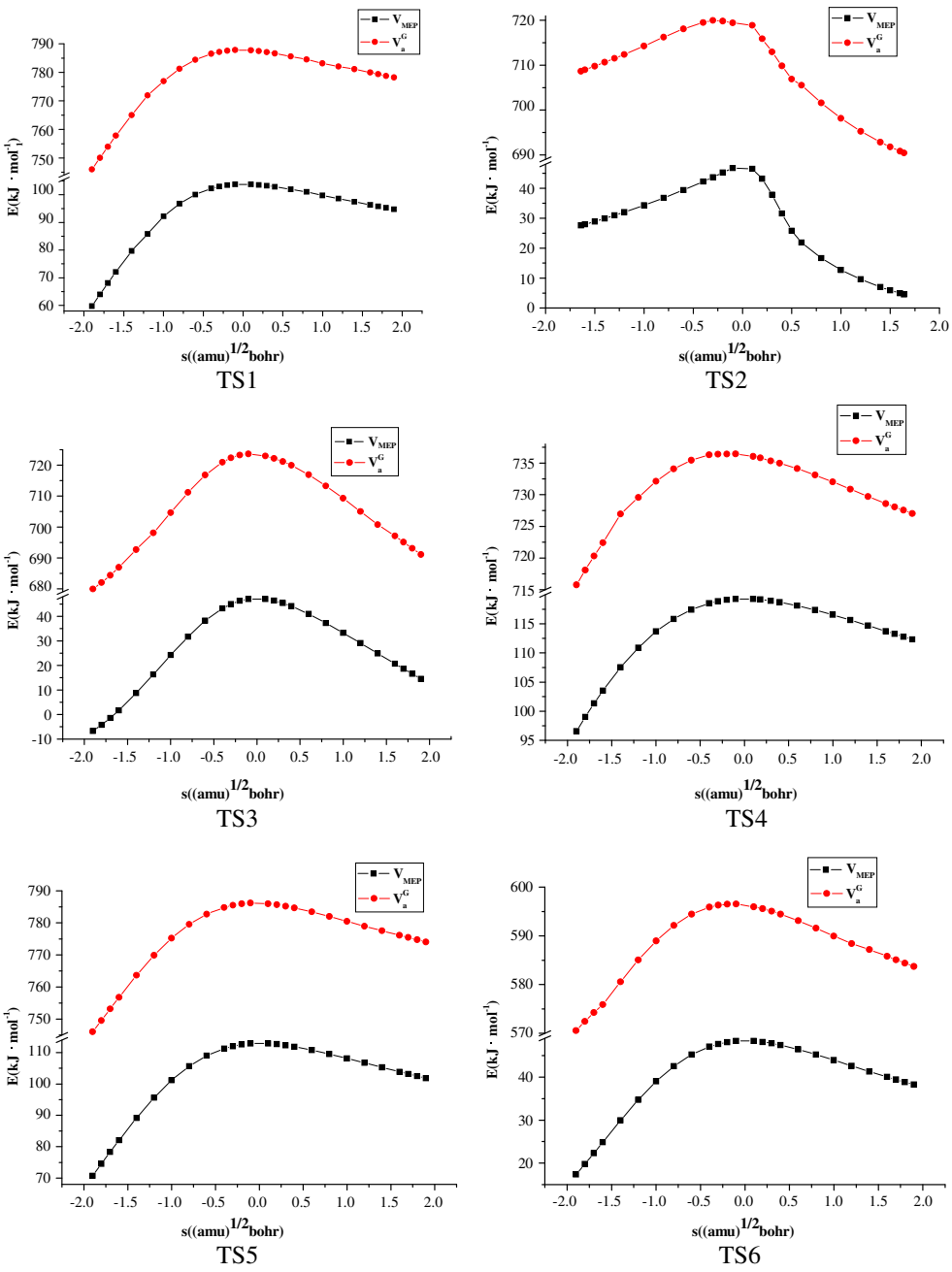

Fig. 3 The classical potential barriers (V_{MEP}) and the vibrationally adiabatic ground state potential energy curve (V_a^G) of the reaction as a function of s (amu)$^{1/2}$ bohr

Fig. 3 (continued)

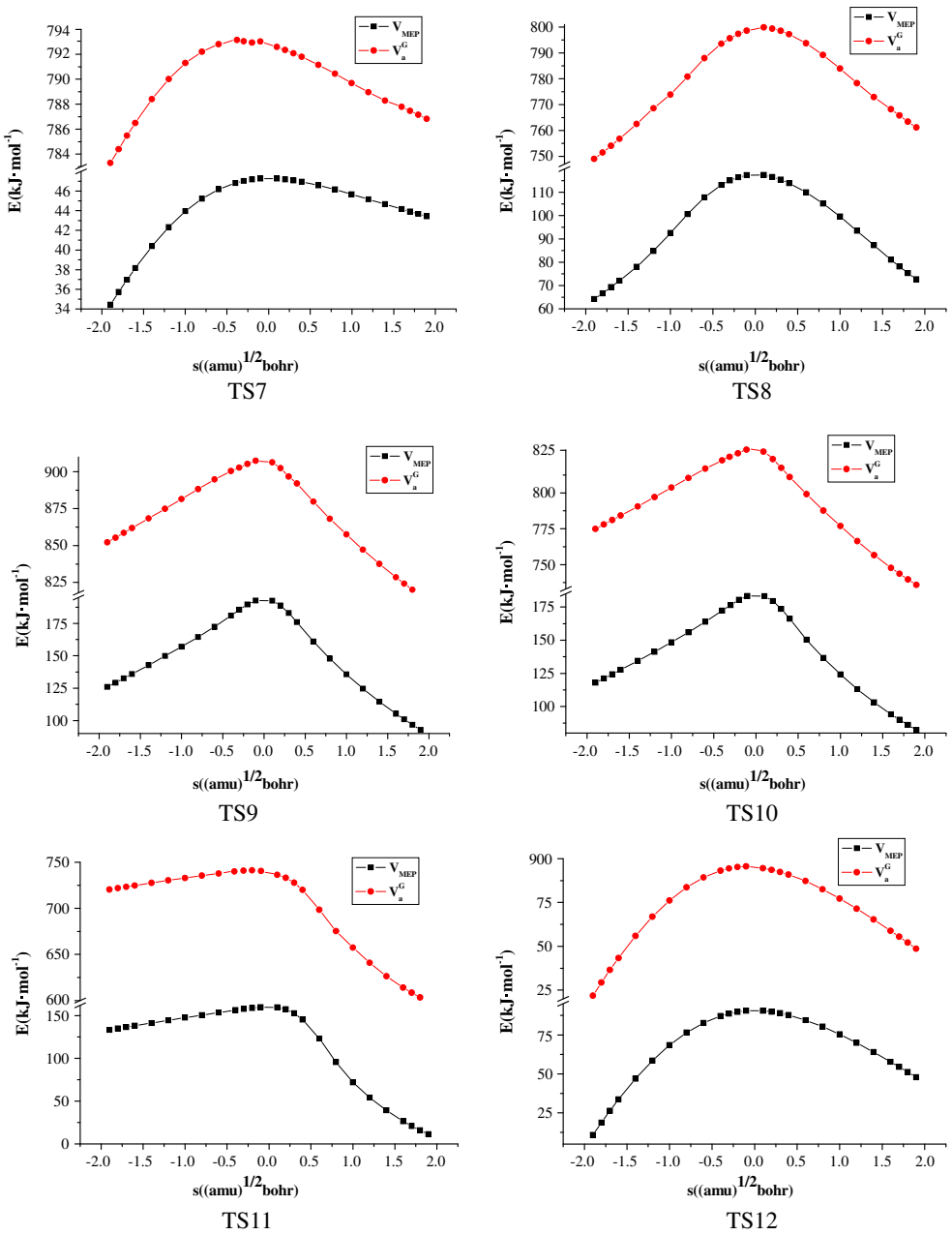

reaction is anticipated to have only a small tunneling effect; on the contrary, the curves are sharper, this type of hydrogen-transfer reaction is anticipated to have an obvious tunneling effect. The vibrationally adiabatic ground state potential energy curve (V_a^G) of the reactions are 95.52, 37.40, 34.06, 108.18, 103.94, 39.93, 132.68, 109.15, 171.18, 163.83, 140.51, 364.15 kJ mol^{-1}, respectively.

Rate constant calculations

The rate constants of all the reactions are calculated by using the TST and TST/Eckart methods based on the B3LYP/6-31G(d) level of theory. The rate constants are shown in Fig. 4.

For the hydrogen transfer reactions (3), (15), (16) and (17), the rate constants calculated by using the TST and TST/Eckart are almost identical at high temperatures (T>500 K), so tunneling effect has little effect at high temperatures, but at low temperatures (500 K>T>200 K), the rate constants calculated by using TST method are different from the TST/Eckart. Along with the decreasing of the temperatures, the deviation is obvious. It is easy to conclude that tunneling effect has a distinct effect on the reactions at low temperatures.

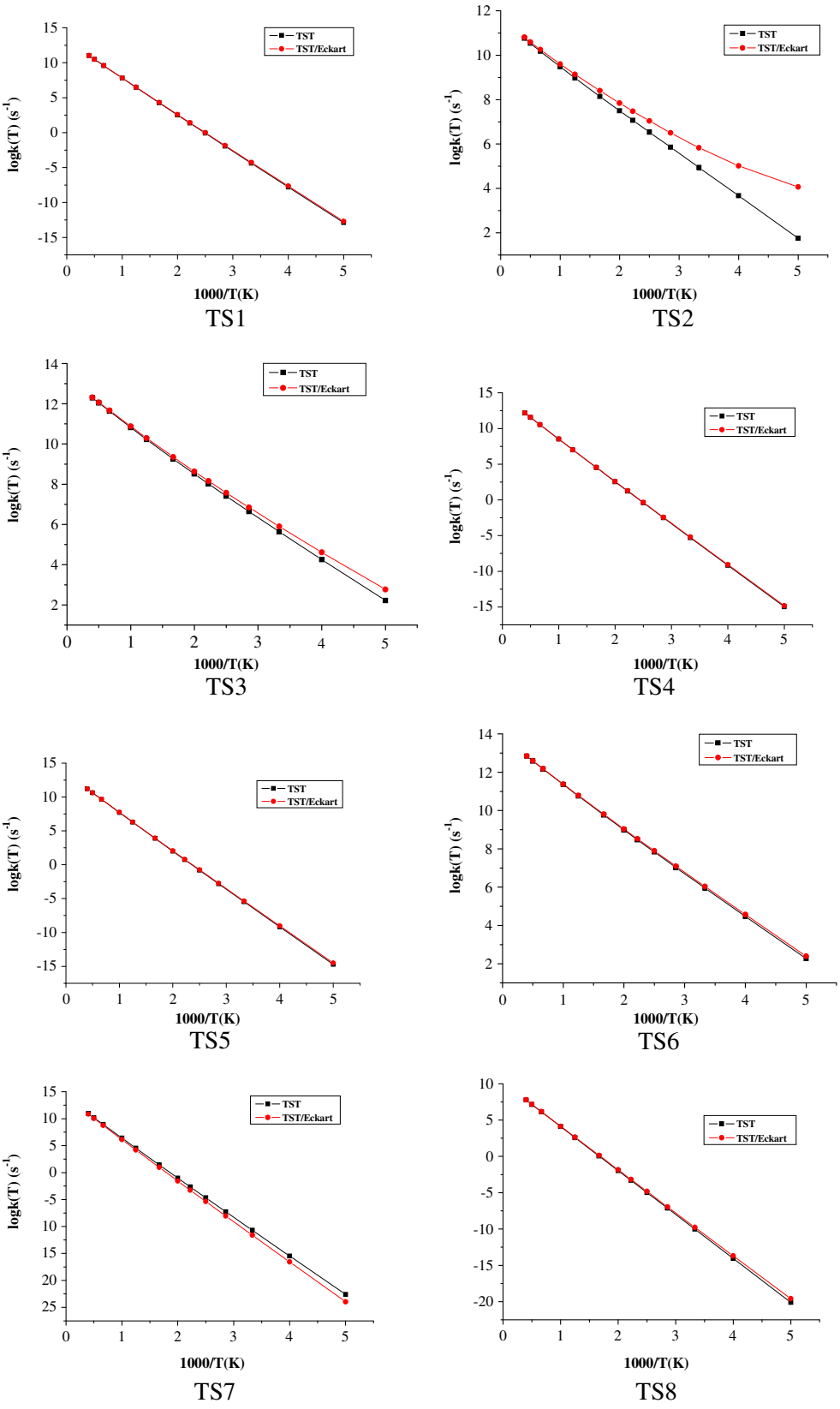

Fig. 4 Arrhenius plot of rate constants calculated at the TST, TST/Eckart levels of theory

For the other reaction, the rate constants calculated by TST and TST/Eckart are almost identical over the whole temperature range. A conclusion we have is that the tunneling effect is unrelated with those reactions not only at low temperatures but also at high temperatures. As it is smooth and this may result in a small tunneling effect over

Fig. 4 (continued)

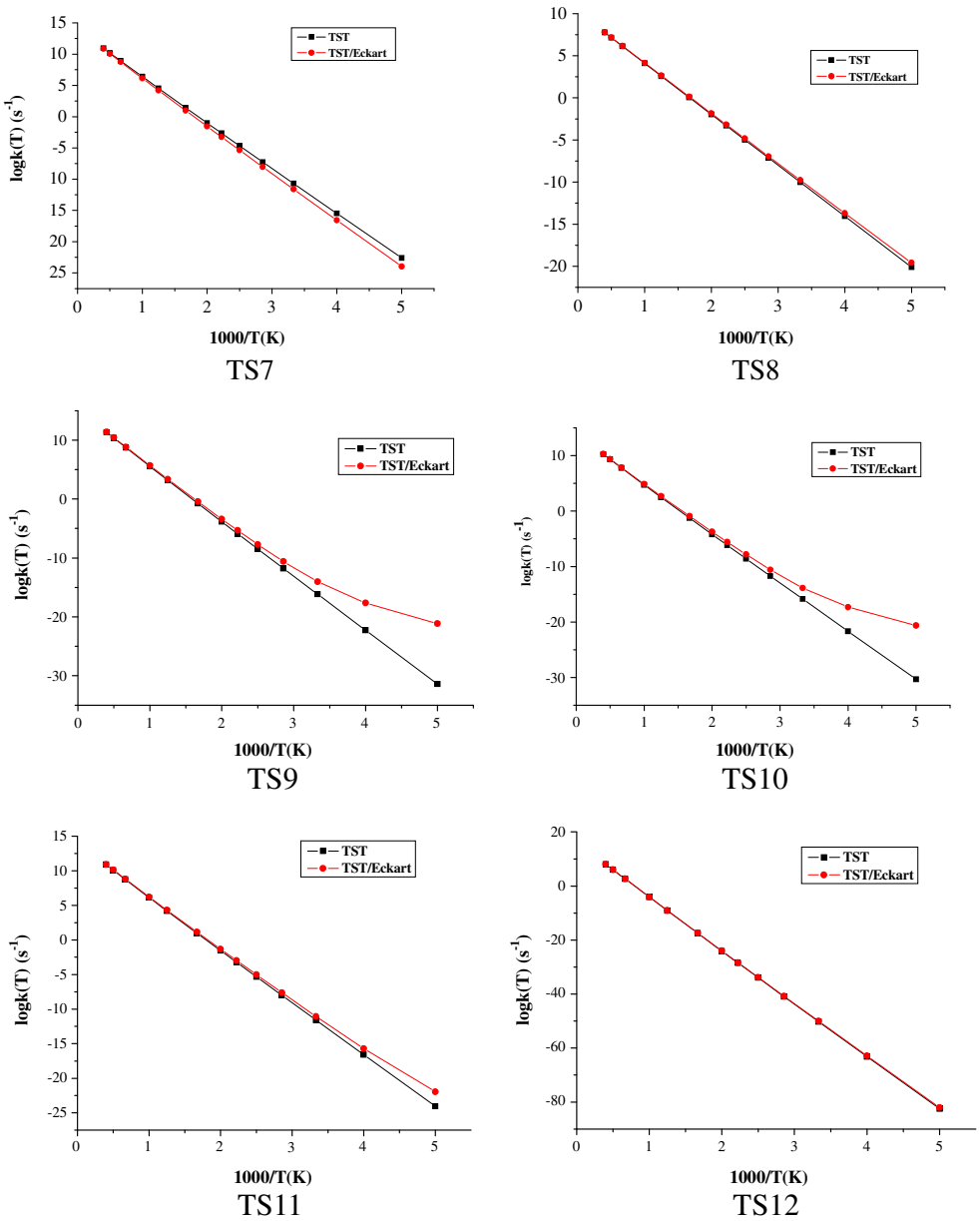

Table 2 The fitted Arrhenius expressions as calculated at the B3LYP/6-31G(d) level of theory

	TST	TST/Eckart
(2)	$k(T) = 1.12 \times 10^{11} \times T^{0.59} \times e^{-(1.17\times10^4/T)} s^{-1}$	$k(T) = 7.60 \times 10^{10} \times T^{0.64} \times e^{-(1.16\times10^4/T)} s^{-1}$
(4)	$k(T) = 1.69 \times 10^{-20} \times T^{2.21} \times e^{-(8.94\times10^3/T)} s^{-1}$	$k(T) = 2.17 \times 10^{-21} \times T^{2.47} \times e^{-(8.56\times10^3/T)} s^{-1}$
(5)	$k(T) = 2.49 \times 10^{12} \times T^{0.62} \times e^{-(1.33\times10^4/T)} s^{-1}$	$k(T) = 2.07 \times 10^{12} \times T^{0.64} \times e^{-(1.32\times10^4/T)} s^{-1}$
(6)	$k(T) = 1.62 \times 10^{11} \times T^{0.66} \times e^{-(1.26\times10^4/T)} s^{-1}$	$k(T) = 1.05 \times 10^{11} \times T^{0.71} \times e^{-(1.25\times10^4/T)} s^{-1}$
(7)	$k(T) = 7.20 \times 10^{11} \times T^{0.55} \times e^{-(5.01\times10^3/T)} s^{-1}$	$k(T) = 6.48 \times 10^{11} \times T^{0.56} \times e^{-(4.95\times10^3/T)} s^{-1}$
(9)	$k(T) = 3.29 \times 10^{10} \times T^{0.97} \times e^{-(1.63\times10^4/T)} s^{-1}$	$k(T) = 3.29 \times 10^{10} \times T^{0.97} \times e^{-(1.69\times10^4/T)} s^{-1}$
(10)	$k(T) = 6.07 \times 10^{9} \times T^{0.11} \times e^{-(1.39\times10^4/T)} s^{-1}$	$k(T) = 8.20 \times 10^{8} \times T^{0.36} \times e^{-(1.35\times10^4/T)} s^{-1}$
(18)	$k(T) = 2.25 \times 10^{10} \times T^{-0.52} \times e^{-(2.37\times10^4/T)} s^{-1}$	$k(T) = 4.37 \times 10^{9} \times T^{-0.32} \times e^{-(2.34\times10^4/T)} s^{-1}$
(3)	$k(T) = 1,26 \times 10^{10} \times T^{0.41} \times e^{-(4.28\times10^3/T)} s^{-1}$	$k(T) = 2.46 \times 10^{4} \times T^{2.05} \times e^{-(2,41\times10^3/T)} s^{-1}$
(15)	$k(T) = 3.78 \times 10^{11} \times T^{1.0} \times e^{-(2.09\times10^4/T)} s^{-1}$	$k(T) = 5.26 \times 10^{-26} \times T^{11.63} \times e^{-(1.12\times10^4/T)} s^{-1}$
(16)	$k(T) = 1.61 \times 10^{10} \times T^{1.02} \times e^{-(1.98\times10^4/T)} s^{-1}$	$k(T) = 3.54 \times 10^{-25} \times T^{11.02} \times e^{-(1.07\times10^4/T)} s^{-1}$
(17)	$k(T) = 5.50 \times 10^{10} \times T^{0.92} \times e^{-(1.70\times10^4/T)} s^{-1}$	$k(T) = 3.93 \times 10^{4} \times T^{2.69} \times e^{-(1.52\times10^4/T)} s^{-1}$

the whole temperature range. The fitted Arrhenius expressions calculated are shown in Table 2.

As a whole, the effects of tunneling effect should be classified into two parts: ①the distinct one for the hydrogen transfer reactions (3), (15), (16) and (17), which will have some effects on the reactions.② the indistinctive one for the other reactions (2), (4), (5), (6), (7), (9), (10) and (18), which can be ignored.

Conclusions

A direct dynamics study for the ingredients RDX in composition B has been carried out by employing the B3LYP/6-31G(d) level of theory. We have postulated three possible pathways for the ingredients RDX in composition B and also found a new low-energy channel which belongs to the N—N fission pathway. Although the N—N bond breaking has higher dissociation energies than the monomer, it is also the initial step. The geometries and harmonic vibrational frequencies of all the stationary points are calculated with the same level of theory. The minimum energy paths are obtained by using the IRC theory with the step length 0.02 $(amu)^{1/2}$·bohr. The rate constants are calculated with TST and TST/Eckart methods. The tunneling effects are remarkable at low temperature (200 K < T < 500 K), which can not be ignored.

Acknowledgments We gratefully acknowledge the National Natural Science Foundation of China, the Program for New Century Excellent Talents in University (No. NCET-09-0051), and the project of State Key Laboratory of Science and Technology (No. YBKT10-03 and No. QNKT11-06).

References

1. Dontsova KMY, Imunek SL, Pennington J, Williford JC, Clint W (2006) J Environ Qual 35:2043–2046
2. Pinto J, Wiegand D (1991) J Hazard Mater 9:205–263
3. Zhao X, Hintsa EJ, Lee YT (1988) J Chem Phys 88:801–803
4. Lee Y, Tang CJ, Litzinger TA (1999) Combust Flame 117:600–628
5. Melius CF (1990) Kluwer, Dordrecht, the Netherlands
6. Harris NJ, Lammertsma K (1997) J Am Chem Soc 119:6583–6589
7. Wu CJ, Fried LE (1997) J Phys Chem A 101:8675–8679
8. Chakraborty D, Muller RP, Dasgupta S, Goddard WA III (2000) J Phys Chem A 104:2261–2272
9. Boyd S, Gravelle M, Politzer P (2006) J Chem Phys 124:104508/1–10
10. Boyd S, Murray JS, Politzer P (2009) J Chem Phys 131:204903/1–7
11. Niu XQ, Zhang JG, Feng XJ, Chen PW, Zhang TL, Wang SY, Zhang SW, Zhou ZN, Yang L (2010) Acta Chim Sinica 69:1627–1638
12. Frisch MJ et al. (2003) Gaussian, Pittsburgh, PA
13. Becke AD (1993) J Chem Phys 98:5648–5652
14. Gonzalez C, McDouall J, Schlegel H (1990) J Phys Chem 94:7467–7471
15. Truhlar D, Isaacson A, Garrett B (1985) Theory of chemical reaction dynamics. CRC, Boca Raton
16. Truong TN, Truhlar D (1990) J Chem Phys 93:1761–1769
17. Zhang SW, Nruong TN (2001) VKLab version 1.0. University of Utah, Utah
18. Chuang YY et al (1999) POLYRATE, program vision 8.2. University of Minnesota, Minneapolis